Available online at www.sciencedirect.com
ScienceDirect
Catalysis Today 130 (2008) 206–220
CATALYSIS TODAY
www.elsevier.com/locate/cattod

Hydroprocessing catalysis on metal sulfides prepared from molecular complexes

Teh C. Ho *

Corporate Strategic Research Labs., ExxonMobil Research and Engineering Co., Annandale, NJ 08801, United States

Available online 22 August 2007

Abstract

This article gives an overview of preparation, characterization, and activity/selectivity of bulk and dispersed metal sulfide catalysts prepared from two families of molecular complexes. New promoter metals are identified. Behavioral features of these molecular-complex-derived catalysts for different hydroprocessing applications are discussed. These catalysts share some common characteristics that make them distinct from conventional Al_2O_3-supported catalysts. Examples are given to show the importance of understanding catalyst–feedstock interactions and balancing catalyst hydrogenation and hydrogenolysis functionalities.

Keywords: Hydrodesulfurization; Hydrodenitrogenation; Hydrogenation; Metal sulfides; Hydroprocessing process; Diesel HDS; Lube hydrotrating; Selectivity

1. Introduction

Hydroprocessing catalysis has been and will continue to be an active research area in the coming years. The key drivers are the tightening environmental regulations, dwindling supply of high-quality crude oils, and growing demands for transportation fuels and lubes. The increasingly large incentive for high-performance catalysts has stimulated the development of novel catalytic materials. A case in point is the recent commercialization of the Nebula catalyst, which is an unsupported (bulk) mixed metal sulfide [1]. Its performance justifies its higher manufacturing cost compared to that of conventional Al_2O_3-supported catalysts.

Bulk metal sulfides have been part of our laboratory's hydroprocessing research portfolio for decades. The first part of this article is a brief review of selected parts of the portfolio whose objective was to develop new catalysts with greater control of activity and/or selectivity relative to conventional catalysts. Specifically, it highlights the preparation and properties of two classes of molecular complexes, which upon thermal decomposition and sulfiding yield highly active and/or selective metal sulfide catalysts for various hydroprocessing applications involving very different feedstock types. Also highlighted are significant observations made in the course of dispersing these catalyst precursors on oxide supports. The exploitation of these molecular-complex-derived catalysts led to the discovery of new synergistic promoter metals that perhaps would not otherwise be identified.

The second part of this article gives an account of kinetic characterization of conventional and experimental catalysts, aiming at gaining a better understanding of process chemistry. The emphasis is on the competition between hydrodesulfurization (HDS) and hydrodenitrogenation (HDN). Examples are given to show the benefit of conducting model-compound experiments alongside with real-feed studies. A case is made for probing reaction dynamics under transient conditions. The results obtained from model-compound and real-feed experiments, taken together, provide insights into the interactions between catalyst hydrogenation/hydrogenolysis functionalities and feedstock composition. The article concludes with a summary of general characteristics of bulk metal sulfide catalysts.

2. Metal amine thiometallates as catalyst precursors

2.1. Bivalent promoter metals

Metal amine thiometallates (MAT) are a family of transition metal/sulfur complexes that have been exploited

* Tel.: +1 908 730 2797; fax: +1 908 730 3344.
E-mail address: teh.c.ho@exxonmobil.com.

0920-5861/$ – see front matter © 2007 Elsevier B.V. All rights reserved.
doi:10.1016/j.cattod.2007.06.076

as hydroprocessing catalyst precursors [2–4]. The compositions of these precursors can be systematically varied. As an example, a doubly promoted system can be represented by $M_xM'_{1-x}(amine)_{6/b}Mo_yW_{1-y}S_4$ in which M and M′ are different bivalent metal promoters, $0 \leq x$, $y \leq 1$, and b is the total number of nitrogen atoms in the amine chelating ligand. The amine ligand used in the present study is ethylenediamine (en) or diethylenetriamine (dien). Examples of M and M′ are Ni, Co, and Fe. The presence of two promoter metals can generate a synergistic effect [5–8]. It is straightforward to extend the synthesis to include more than two promoter metals. The preparation of the MAT-based bulk catalysts does not involve calcination in air; the final catalysts are obtained from thermal decomposition of MAT in a sulfur-bearing stream (e.g., 10% H_2S in H_2) at temperatures typically between 320 and 400 °C. Varying decomposition procedures would lead to different catalytic properties. After the decomposition and sulfiding treatment, the bulk metal sulfides generally contain small amounts of carbon and nitrogen. The BET (with N_2) surface areas of the resulting bulk catalysts typically range between 5 and 15 m^2/g.

Many of the MAT-derived bulk sulfide catalysts have higher volumetric HDS and/or HDN activities than commercial sulfided $CoMo/Al_2O_3$ and $NiMo/Al_2O_3$ catalysts [2–11]. This family of catalysts shows a strong effect of metal composition. For illustration, Fig. 1 shows that the HDN activity of the FeMo sulfide catalyst can be significantly increased by copromotion with Ni or Co [6]. These doubly promoted molybdenum sulfides are more effective for HDN than their singly promoted counterparts. Activity and selectivity data were obtained in tests with light catalytic cycle oil (LCO), a most refractory class of feedstocks rich in aromatics and five-membered ring nitrogen heterocycles such as alkylcarbazoles [5].

We next explore the extent to which the foregoing strong metal composition effect can be carried over to trivalent chromium as a promoter or copromoter.

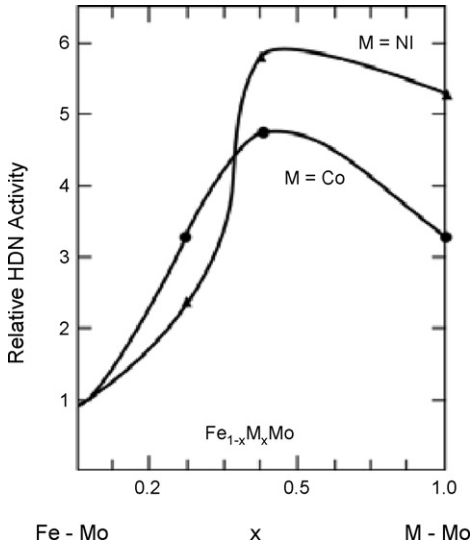

Fig. 1. Effects of metal composition on relative HDN activities of $Fe_{1-x}Ni_xMo$ (▲) and $Fe_{1-x}Co_xMo$ (●) sulfides.

2.2. Bulk Cr-promoted catalysts

To extend the synthesis to include chromium, some modifications are necessary. This leads to two routes for preparing chromium-containing catalysts [8–11]: one involves the aforementioned chelation chemistry; the other is related to the olation process [12]. In the former case, the formation of chromium–amine thiomolybdate salt is not kinetically favored over hydrolysis. So an essential step in the chelation route entails isolating Cr^{3+} via the formation of $Cr(en)_3Cl_3$ in a non-aqueous environment. This is done by slowly adding anhydrous $CrCl_3$ to en, resulting in a yellow precipitate which is filtered and recovered. $Cr(en)_3Cl_3$ is soluble and stable in water, so $[Cr(en)_3]_2(MoS_4)_3$ can be prepared by metathesis in the presence of en, leading to an orange-red precipitate, as summarized below [8–10].

$$Cr(en)_3Cl_3 + 1.5(NH_4)_2MoS_4 \rightarrow Cr(en)_3(MoS_4)_{1.5}\downarrow + 3NH_4Cl \quad (1)$$

The synthesis involving olation is illustrated by the following example. Forty grams of ammonium thiomolybdate $(NH_4)_2MoS_4$ was dissolved into 82 ml of dien. The resulting dark red solution was cooled to 0 °C in an ice bath. In a separate flask, 27.56 g of $Cr(OH)_3{\cdot}6H_2O$ was dissolved into 250 ml of distilled water. To this solution was added dien, leading to the formation of a precipitate. The resulting slurry was allowed to stand for 2–3 h and then added slowly to the $(NH_4)_2MoS_4$/dien solution. This resulted in the formation of a bright orange precipitate which was separated by filtration, washed with water and ethanol and dried at ambient temperature under vacuum. Ninety-one grams of the catalyst precursor was obtained, with the empirical formula $[Cr(OH)_3{\cdot}1.5H_2O](H_2dien)_{1.1}(MoS_4)_{1.1}$.

The Cr-containing catalysts prepared from the olation route were tested with LCO at 325 °C and 3.15 MPa (8–10). Their relative (hence dimensionless) volumetric HDS and HDN activities and selectivities are compared with those of commercial Al_2O_3-supported CoMo and NiMo catalysts (Catalysts A and B, respectively) and those of the MAT-derived bulk FeMo catalyst. Table 1 summarizes the results. The HDN selectivity is defined as the ratio of the rate constant of HDN to that of HDS, that is, $S_N = k_{HDN}/k_{HDS}$. Referring to Table 1, the HDN activity of Cr-containing catalysts can be significantly increased by copromotion with Ni or Fe, whereas their HDS activity can be promoted by Co. For reference, also shown in Table 1 is the bulk FeMo catalyst. Comparing the present results with those in Fig. 1 indicates that there exists a synergism between Cr and Fe as copromoters, an important finding to which we will refer again. Catalysts prepared from the chelation route show similar trends, with their activities being somewhat lower than those shown in Table 1 [8,11].

The foregoing results indicate that the MAT-derived catalysts give rise to an unusual combination of high HDN and low HDS compared to commercial supported catalysts. This appears to be a general characteristic of many bulk metal sulfides. To put this observation in perspective, we next

Table 1
Relative activity and selectivity of bulk catalysts

Catalyst	k_{HDN}	k_{HDS}	S_N
$CoMo/Al_2O_3$ (A)	0.44	1.0	0.44
$NiMo/Al_2O_3$ (B)	1.00	0.93	1.08
Fe-Mo	0.94	0.16	5.88
Cr-Mo	3.17	0.22	14.4
$Cr_{0.5}$-$Ni_{0.5}$-Mo	7.86	1.87	4.20
$Cr_{0.7}$-$Ni_{0.3}$-Mo	7.14	1.56	4.58
$Cr_{0.5}$-$Fe_{0.5}$-Mo	5.87	0.38	15.45
$Cr_{0.5}$-$Co_{0.5}$-Mo	1.43	1.64	0.87

establish a framework for probing this characteristic on a formal basis.

3. HDS–HDN selectivity trajectory

3.1. Kinetic analysis

Studies have indicated that active sites on Mo/W-based metal sulfide catalysts are sulfur vacancies associated with exposed Mo/W cations and SH^-/S^{2-} groups on the MoS_2/WS_2 edge [13]. The electronic and structural configurations of these coordinatively unsaturated sites are also influenced by promotes such as Co and Ni located at edge sites as substituted metals. The formation of vacancies is enhanced if the vacancy is shared by Co and Mo. All of these sites can perform HDS, HDN, and hydrodearomatization (HDA) with varying degrees of activities and selectivities. For kinetic modeling, it is customary to lump those sites into either a single site or two sites (hydrogenation and hydrogenolysis).

Let S, N, and A be the concentrations of total sulfur, nitrogen, and aromatics in the oil at any point in a steady state plug-flow reactor of length L, respectively. The feed sulfur, nitrogen and aromatic concentrations are S_f, N_f, and A_f. Also let $\tau = z/L$ be the dimensionless distance variable with z being the reactor axial coordinate and LHSV be the liquid hourly space velocity. Assuming that the catalyst surface is Langmurian and all reactants compete for the same type of active site, the mass balance equations for S and N take the form

$$\mathrm{LHSV}\frac{\mathrm{d}S}{\mathrm{d}\tau} = -\frac{k_s S^n}{F(S,N,A)} \tag{2}$$

$$\mathrm{LHSV}\frac{\mathrm{d}N}{\mathrm{d}\tau} = -\frac{k_n N}{F(S,N,A)} \tag{3}$$

where $F(\tau)$ is the inhibition term which may take the form $F = (1 + K_n N + K_s S + K_a A)^m$ for a single-site model or $F = (1 + K_{n1} N + K_{s1} S + K_{a1} A)^l (1 + K_{n2} N + K_{s2} S + K_{a2} A)^u$ for a two-site model. The exponents m, l, and u are positive numbers. The K's in F are inhibition constants, whereas k_s and k_n are lumped rate constants for HDS and HDN, respectively. Depending on the rate-limiting step (e.g., adsorption or surface reaction), k_s and k_n assume different physical meanings [14]. In general, $n \geq 1$. At the reactor inlet $\tau = 0$, $S = S_f$ and $N = N_f$, whereas at the reactor outlet $\tau = 1$, $S = S_p$ and $N = N_p$. A tacit assumption here is that the reactor hydrogen pressure is approximately constant. As such, the hydrogen pressure dependence is embedded in k_s and k_n.

Eqs. (2) and (3) imply that the influence of the inhibition term on all reactants (sulfur, nitrogen, and aromatics) is the same. This uniform inhibition assumption has two consequences. The first is that one can simplify the analysis of the system behavior by using a wrapped time scale θ defined as $\mathrm{d}\theta(\tau) = F^{-1}\mathrm{d}\tau$ with $\theta(0) = 0$. Eqs. (2) and (3) can then be rewritten as $\mathrm{LHSV}(\mathrm{d}S/\mathrm{d}\theta) = -k_s S^n$ and $\mathrm{LHSV}(\mathrm{d}N/\mathrm{d}\theta) = -k_n N$. This says that on the warped time scale, S and N disappear as if they were independent, one following a pseudo-nth-order kinetics, while the other pseudo-first-order kinetics.

The second consequence gives a simple physical picture of how S and N interact. Dividing Eq. (2) by Eq. (3) and performing the integration from the reactor inlet to outlet yield an explicit relation between the extents of HDS and HDN. The $n = 1$ case gives a power-law relation: $S_p/S_f = (N_p/N_f)^p$ where $p = k_s/k_n$ is a selectivity factor depending on temperature and hydrogen pressure. Thus,

$$\ln\left(\frac{S_p}{S_f}\right) = p\ln\left(\frac{N_p}{N_f}\right) \tag{4}$$

For a given feedstock, plotting $\ln(S_p/S_f)$ versus $\ln(N_p/N_f)$ over a range of reaction severities (e.g., different LHSVs) generates a selectivity trajectory, which is a straight line with slope p if p is constant. The shape of the trajectory remains unchanged whether the time scale is warped or not. We define $\ln(S_p/S_f) = \ln(N_p/N_f)$ as the selectivity parity line ($p = 1$) on which the catalyst is regarded as equally selective toward HDS and HDN. When $p > 1$, the catalyst is called HDS-selective.

For $n > 1$, it can be shown that

$$(1-n)\ln\left(\frac{S_p}{S_f}\right) = \ln\left[1 + \frac{p(1-n)}{S_f^{1-n}}\ln\left(\frac{N_p}{N_f}\right)\right] \tag{5}$$

It follows that that the selectivity trajectory is concave upward, a mathematical consequence of the fact that the pseudo-reaction-order of HDS is higher than that of HDN ($n > 1$). As a result, the HDS rate, being more sensitive to concentration, decreases more rapidly than the HDN rate as both reactions proceed (this can easily be seen on the warped time scale). Mechanistically, as will become apparent later (Section 7.1.3), what goes on is that sulfur removal reactions become increasingly more inhibited by nitrogen species as the HDS level gets deeper and deeper.

The trajectory becomes approximately linear when the following condition is met

$$\frac{\text{HDN rate}}{\text{HDS rate}} \approx \frac{k_n}{k_s S_f^{n-1}} \gg (n-1)\ln\left(\frac{N_f}{N_p}\right) \tag{6}$$

The pseudo-straight-line trajectory is described by

$$\ln\left(\frac{S_p}{S_f}\right) \approx \bar{p}\ln\left(\frac{N_p}{N_f}\right) \tag{7}$$

where $\bar{p} = k_s S_f^{n-1}/k_n$ in which $k_s S_f^{n-1}$ can be regarded as an equivalent first-order rate constant for HDS. Eq. (6) reveals that a highly HDN-selective catalyst ($\bar{p} \ll 1$) is more likely to give

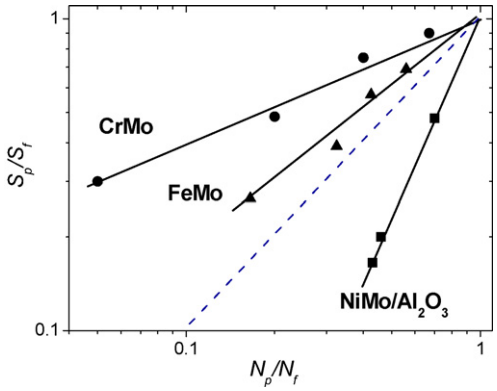

Fig. 2. HDN/HDS selectivity trajectories, $\ln(S_p/S_f)$ vs. $\ln(N_p/N_f)$, for bulk FeMo and CrMo (olation route) catalysts as well as commercial $NiMo/Al_2O_3$ catalyst. The dotted line means equal selectivity.

rise to a pseudo-straight-line trajectory (see Fig. 2). When n is close to unity, the trajectory is almost linear; Eq. (6) is trivially satisfied when $n = 1$.

3.2. HDN-selective catalysts

The forgoing analysis provides a norm for analyzing HDS–HDN interactions by plotting $\ln(S_p/S_f)$ versus $\ln(N_p/N_f)$ for a given feedstock over different catalysts or for a given catalyst with different feedstocks at the same reaction conditions. Fig. 2 contrasts the selectivity trajectories of bulk FeMo and CrMo sulfide catalysts with that of a commercial sulfided $NiMo/Al_2O_3$ catalyst (Catalyst B), the latter in general being more HDN-selective than $CoMo/Al_2O_3$. The experiments were done with LCO at 325 °C and 3.15 MPa H_2 pressure with varying LHSV. All these catalysts give rise to straight-line trajectories (more on this in Section 7.1.3). Below the selectivity parity (dotted) line is the HDS-selective region in which the $NiMo/Al_2O_3$ catalyst lies. In contrast, the FeMo and CrMo catalysts lie above the parity line. This result may seem surprising given the perception that HDN is more difficult than HDS (the C–N bond is in general stronger than the C–S bond in an aromatic ring); a corollary of this is to say that FeMo and CrMo lie in a ''forbidden'' region. It appears that MAT-derived bulk sulfides enable one to exploit a wider region within the HDS–HDN space than previously thought possible.

Fig. 2 and similar plots indicate that it pays to look at a catalyst's selectivity toward certain hydroprocessing reactions and thereby gain a better understanding of how different hydroprocessing reactions (e.g., HDS versus HDN) interact with each other. An HDN-selective catalyst generally implies a high hydrogenation functionality [7]. To a first approximation, Fig. 2 may be regarded as gauging a catalyst's hydrogenation function relative to its hydrogenolysis function. Removing sulfur from refractory sulfur heterocycles such as 4-substituted and 4,6-disubstituted dibenzothiophenes places a premium on catalyst's hydrogenation functionality [15]. The consideration of catalyst selectivity can also suggest process options. For example, an HDN-selective catalyst can be used synergistically with an HDS-selective catalyst in a stacked bed for maximum overall activity [15]. Such a process may also result in savings in overall hydrogen consumption. A primary requirement in hydrocracking is the selective removal of nitrogen compounds to protect downstream catalysts. An HDN-selective catalyst is also needed in manufacturing lubricating oils. For good oxidation stability, it is necessary to remove nitrogen species (proxidants) while leaving behind sulfur species (antioxidants). MAT-derived Cr-containing bulk sulfides are better lube hydrotreating catalysts than conventional catalysts [16].

4. Characterization of bulk sulfides

Fig. 3 shows the start-of-the-run (SOR) data on the bulk FeMo catalyst prepared from bis(diethylenetriamine) iron thiomolybdate [17]. The test was done in a fixed-bed reactor with LCO at 325 °C and 3.15 MPa. It took about 300 h for the HDN level to line out, whereas the HDS level lined out shortly after reactor startup. Apparently, during the SOR period the catalyst undergoes some changes that affect HDN more than HDS.

The FeMo catalyst was characterized before and after the SOR period using a high-resolution scanning transmission electron microscope (STEM) coupled with energy dispersive microanalysis and microdiffraction [17]. As shown in Fig. 4A, the dominant phase in the fresh catalyst is basically amorphous in nature with occasional appearance of single or double lines with about 6.2 Å in spacing. The amorphous nature can also be seen in the corresponding microdiffraction pattern (inset). Referring to Fig. 4B, the minor phase also shows single or double-layer MoS_2-like structures (about 6.2 Å spacing). The corresponding microdiffraction pattern (inset) identifies both the MoS_2-like crystalline spots and the amorphous diffraction ring. The crystalline diffraction spots are quite diffuse in intensity, indicative of a poorly crystalline phase. X-ray elemental analysis using a 100 Å probe size indicates that the

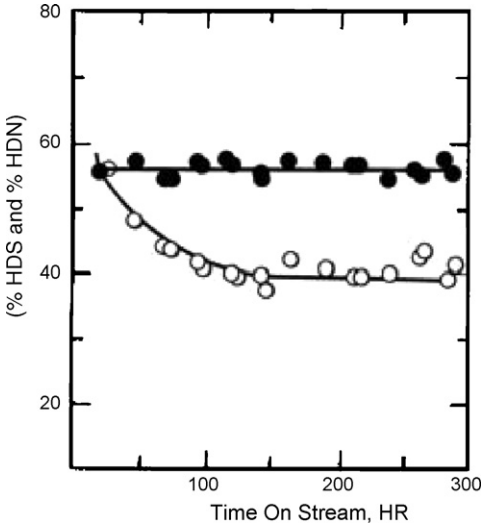

Fig. 3. Percents of HDS (●) and HDN (○) vs. on-stream time (hour) for bulk FeMo catalyst prepared from MAT; LCO; 325 °C, 3.15 MPa, 4.0 LHSV, 3000 SCF/B H_2.

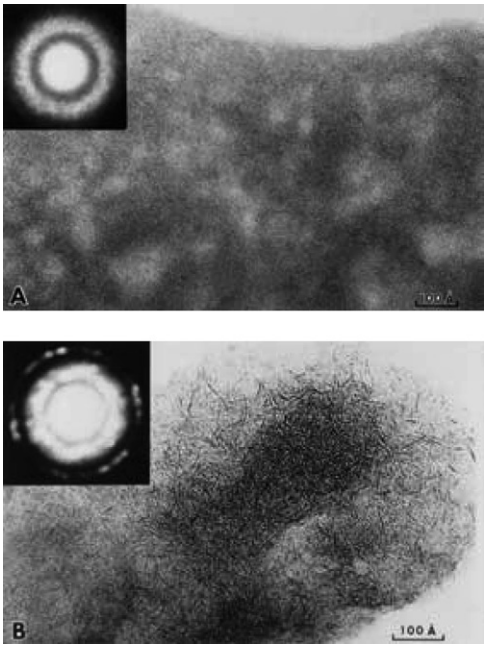

Fig. 4. Transmission electron micrograph of fresh FeMo catalyst showing (A) predominantly amorphous phase, which is the major phase and (B) single and double-layer MoS_2-like structure, which is the minor phase.

fresh catalyst is chemically homogeneous within the 100 Å spatial resolution.

While on oil, a small fraction of the initial single amorphous phase locally becomes converted into two separate phases consisting of small iron sulfide particles (identified as pyrrhotite $Fe_{1-x}S$) and the surrounding MoS_2-like phase. Fig. 5 shows the STEM micrograph of lined-out FeMo catalyst. The arrows mark small $Fe_{1-x}S$ crystallites. The microdiffraction pattern (inset) taken from the Mo-rich FeMo sulfide indicates that this MoS_2-like phase shows a much more well-defined crystalline structure than that in Fig. 4B. Presumably, the HDN activity decreases as the phase separation proceeds. The phase separation becomes progressively slower as the separation proceeds, probably because $Fe_{1-x}S$ is gradually encapsulated by the MoS_2-like phase which inhibits further growth of $Fe_{1-x}S$. Unlike the fresh catalyst, the lined-out catalyst showed

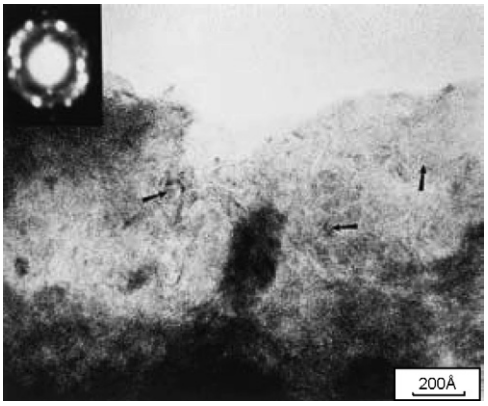

Fig. 5. Transmission electron micrograph of lined-out FeMo catalyst showing the details of the constituent phases. Arrows indicate some of the $Fe_{1-x}S$ crystallites.

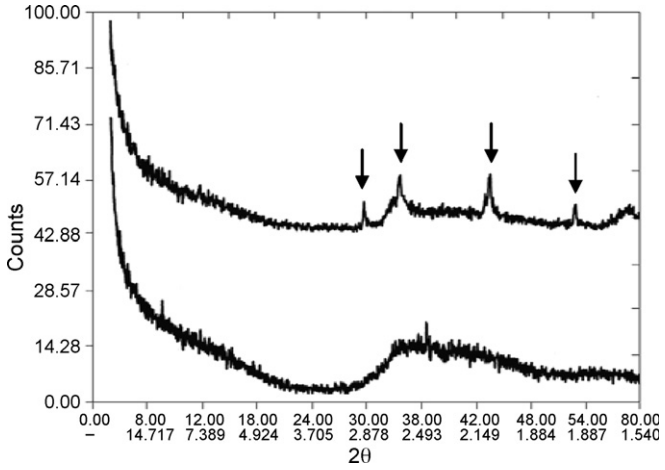

Fig. 6. X-ray powder diffraction patterns of lined-out bulk FeMo (upper pattern) and CrMo (lower pattern) catalysts prepared from MAT. The arrows indicate $Fe_{1-x}S$.

evidence of phase separation and chemical inhomogeneity. Notwithstanding all this, the major phase is basically amorphous in nature.

Fig. 6 compares the X-ray powder diffraction patterns of spent bulk FeMo and CrMo catalysts [8]. The FeMo catalyst shows a poorly crystalline MoS_2 superimposed with ''sharp'' lines of $Fe_{1-x}S$. In contrast, the CrMo catalyst exhibits only an amorphous phase, which apparently is more stable than that in the FeMo catalyst. In either case, the absence of the (0 0 2) peak at $2\theta = 14.4^\circ$ indicates very low MoS_2 stacking, consistent with the single or double-layer features identified by STEM. These bulk sulfide catalysts demonstrate that Type II sites [13] can be as short as one or two layers.

5. Catalyst precursors composited with colloidal oxides

As mentioned, the surface areas of MAT-derived metal sulfide catalysts are very low. Moreover, the MAT compounds are virtually insoluble in conventional solvents. From the standpoint of metal utilization, a non-impregnation method should be developed for dispersing MAT onto an oxide. What follows is an approach addressing this point using colloidal oxides as supports or dispersants [9].

5.1. Preparation

The approach is to prepare a composite of an MAT compound and a colloidal oxide through gel formation. The preparation was typically carried out as follows. The required amount of oxide sol was added to a large three-neck flask and diluted to three–five times its volume with deionized water. While vigorously stirring the aquasol with a mechanical stirrer, the alkaline thiomolybdate solution (either en or dien) was added slowly. At some point during the addition, gel formation occurred. If necessary, the gel was broken up with a spatula and addition of small amounts of water, until stirring could be resumed. The addition of thiomolybdate was then completed. While continuing to stir the thiomolybdate-oxide mixture

vigorously, a solution of promoter metal–amine complex ions [$Ni(en)_3^{+2}$, $Co(en)_3^{+2}$, $Cr(en)_3^{+3}$] or promoter metal–aquo complex ions [$Fe(H_2O)_n^{+2}$, $Mn(H_2O)_n^{+2}$] was added from a dropping funnel in order to precipitate the corresponding metal–amine complex thiomolybdate (or thiotungstate) on the oxide gel. The composite material was then recovered by filtration, washed and dried in vacuum at 50 °C.

If either en or dien is added to aqueous solutions of ferrous or manganous ions, the corresponding hydroxide precipitates, due to hydrolysis, that is,

$$Fe(H_2O)_6^{2+} + en \rightarrow Fe(OH)_2enH_2^{2+} + 4H_2O \quad (8)$$

If instead, the aquo complex ions are added to aqueous thiomolybdate containing en or dien, as described in the above procedure, the formation of the corresponding metal–amine complex thiomolybdate is kinetically favored, namely that

$$Fe(H_2O)_6^{2+} + 3en + MoSO_4^{2+} \rightarrow Fe(en)_3MoS_4 \downarrow + 6H_2O \quad (9)$$

However, $Fe(en)_3MoS_4$ and $Mn(en)_3MoS_4$ are unstable in pure water, and must be washed with aqueous amine. By contrast, the corresponding dien complex salts are stable to water washing.

To summarize, preparations of $Ni(en)_3MoS_4$, $Ni(en)_3WS_4$, $Cr(en)_3(MoS_4)_{1.5}$, $Fe(en)_3MoS_4$, and $Mn(en)_3MoS_4$ were carried out in the presence of colloidal Al_2O_3, Cr_2O_3, and Fe_2O_3 by the procedure described above. Prior to activity tests, these composite precursors were decomposed at 325 °C for 3 h in flowing 10% H_2S/H_2 to produce final catalysts.

5.2. Fe-Cr synergism

As before, the activity tests were done with LCO. Table 2 summarizes relative HDS and HDN volumetric activities and selectivities of MAT-derived catalysts composited with colloidal Cr_2O_3 (5 μm, 450 m^2/g surface area). The reference catalysts are Catalysts A and B.

As can be seen, all Cr_2O_3-composited MAT catalysts have higher HDN volumetric activities than Catalyst B. The $Fe(en)_3MoS_4/Cr_20_3$-derived catalyst, the most HDN-selective catalyst, is more active for HDN than either bulk FeMo or CrMo sulfide (Table 1), indicating an Fe-Cr synergism. By contrast, CrMo on colloidal Fe_20_3 showed no HDN activity at all.

The high HDN activity and selectivity of the $Fe(en)_3MoS_4/Cr_20_3$-derived catalyst prompted us to characterize its structure.

Table 2
Relative volumetric activities of MAT/Colloidal Cr_2O_3 catalysts

Catalyst/precursor	k_{HDN}	k_{HDS}	S_N
Catalyst A	0.44	1.0	1.08
Catalyst B	1.00	0.93	1.08
$Ni(en)_3MoS_4$	1.88	0.27	6.96
$Ni(en)_3WS_4$	2.48	0.39	6.36
$Fe(en)_3MoS_4$	4.63	0.31	14.93
$Cr(en)_3(MoS_4)_{1.5}$	3.40	0.81	4.20
$Mn(en)_3MoS_4$	1.68	0.20	8.4

Table 3
Sulfur analysis of used chromia supported catalysts

Catalyst	Calculated %S	Measured %S
$Ni\text{-}Mo/Cr_2O_3$	18.00	17.80
$Fe\text{-}Mo/Cr_2O_3$	10.96	32.39

Neither the fresh composited precursor [$Fe(en)_3MoS_4/Cr_2O_3$)] nor the decomposed (325 °C, 10% H_2S in H_2 for 3 h) composited catalyst showed any crystalline peaks by XRD. This suggests good dispersion of the precursor on the chromia support. A sample of used FeMo-on-chromia catalyst was further characterized by STEM and EDAX. No evidence of crystalline MoS_2 was observed. Some crystallinity was observed in the Fe-rich portions of the specimen, indicating the presence of some iron sulfide. Surprisingly, the sample appears to be sulfur-rich based on EDAX analysis. In fact, the intensity of the sulfur peak is too great to be associated solely with the Fe and Mo present in the catalyst. It is likely that the chromia support has been sulfided.

Further evidence of sulfiding of the chromia support was obtained by wet sulfur analysis of used catalysts. As shown in Table 3, the actual sulfur content of the composite $NiMo/Cr_2O_3$ catalyst is very close to the calculated value based on the assumption that Cr is present solely as Cr_2O_3. For the $FeMo/Cr_2O_3$ catalyst, however, the measured sulfur is three times the calculated value, indicating conversion of chromia to chromium sulfide. Finally, the XRD pattern of the lined-out chromia-composited FeMo catalyst (100 h on oil) shows some small crystalline peaks, which were identified as Cr_2S_3, as shown in Fig. 7.

Thus, in the FeMo/chromia case, there is strong evidence that the chromia support is extensively sulfided during decomposition with a H_2S-in-H_2 gas mixture. The presence of Cr_2S_3 is believed to play a key role in promoting the HDN activity and selectivity of the FeMo/chromia-derived catalyst.

6. Metal amine metallates as catalyst precursors

The preparation of MAT involves using hydrogen sulfide as a reagent (e.g., preparation of ammonium thiomolybdate). It is

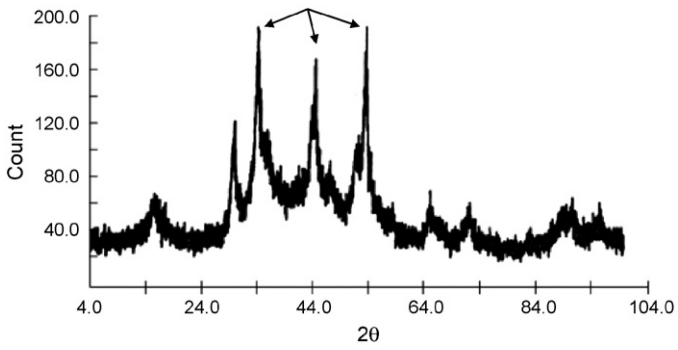

Fig. 7. X-ray powder diffraction pattern of lined-out colloidal Cr_2O_3-composited MAT-derived FeMo catalyst. Crystalline Cr_2S_3 is identified (indicated by arrows).

highly desirable to prepare MAT-like catalyst precursors in the absence of H_2S. This naturally points to MAT's cousin compounds—metal amine metallates (MAM). This class of heterometallic metal oxygen complexes can be prepared from metal chlorides or nitrates and ammonium molybdate or tungstic acid by precipitation of the product in methanol or in aqueous ethylenediamine [18]. Many metal amine molybdates, e.g., $Co(en)_3MoO_4$, $Ni(en)_3MoO_4$, $Cr(en)_3(MoO_4)_{1.5}$, are soluble and stable in water; they can be supported on high surface area oxides via impregnation.

6.1. Sulfiding behavior

The MAM materials upon sulfiding with H_2S/H_2 at elevated temperatures yield poorly crystalline metal sulfides having higher BET surface areas (ca. 60–100 m^2/g) than those derived from MAT. Gas sulfiding of MAM with H_2S is a rather facile reaction even at low temperatures (~200 °C). It is accompanied by a significant temperature rise, making it difficult to ascertain the true conditions at which the catalyst is sulfided. To help control the sulfiding operation, a mathematical model predicting the extent of hot spotting and the speed of traveling exotherm in a fixed-bed reactor was developed [19]. Fig. 8 shows the traveling temperature profiles as a function of sulfiding time for the $Co(en)_3MoO_4$-derived catalyst. With the 10%-H_2S-in-H_2 gas mixture as the sulfiding agent, the bulk CoMo catalyst gives rise to a severe hot spotting, far more so than conventional catalysts [20]. As a result, the particle temperature is higher than the gas temperature, which in turn is higher than the reactor wall temperature. The activity and selectivity of the bulk CoMo catalyst are sensitive to H_2S partial pressure during sulfiding [21]. When developing new catalysts, one should keep in mind that each catalyst is different. Its presulfiding protocol should be carefully tailored to avoid underutilization of catalyst's active ingredients.

6.2. Hydrodearomatization

Testing of bulk catalysts prepared from $Ni(en)_3MoO_4$, $Ni_{0.5}Mn_{0.5}(en)_3MoO_4$ (hereafter denoted as NiMnMo), and $Mn(en)_3MoO_4$ identified a synergism between Ni and Mn as copromoters [15]. The bulk NiMnMo catalyst is HDN-selective. It desulfurizes 4,6-diethyldibenzothiophene (46DEDBT) faster than it desulfurizes dibenzothiophene (DBT) [15]. Characterization of NiMnMo indicates that poorly crystalline MoS_2 particles are largely present as three and four slabs, with an average stacking number of 3.6 [15]. In what follows, we use the bulk NiMnMo sulfide as an HDA catalyst for treating a highly aromatic feedstock.

6.2.1. Temperature excursion

The bulk NiMnMo catalyst was tested against a commercial $CoNiMo/Al_2O_3$-SiO_2 catalyst (Catalyst C) in two independent fixed-bed reactors using LCO as the feed. Each reactor was heated in a sandbath. Fig. 9 compares the relative (hence dimensionless) HDA rate constants for the NiMnMo catalyst and Catalyst C as functions of H_2 pressure at 650 °F, 0.86 LHSV, and 3000 standard cubic feet H_2/barrel oil (SCF/B). The NiMnMo not only has a much higher activity but also a stronger H_2 pressure dependence.

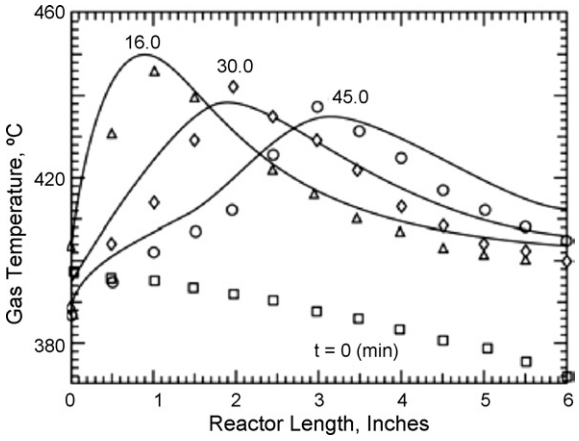

Fig. 8. Experimental and predicted gas temperature profiles along a fixed-bed reactor at different sulfiding times (16, 30, and 45 min) for a bulk MAM-derived CoMo catalyst.

It must be pointed out that the data at 1200 psig should be used with caution because they are clouded by a significant temperature rise observed with the NiMnMo catalyst, owing to its high hydrogenation activity. Fig. 10 depicts the reactor axial temperature profiles observed with NiMnMo and Catalyst C. While the exact extent of the hot spotting is unclear, the existence of a significant axial temperature gradient is evident for the NiMnMo catalyst. The maximum temperature rise is at least 27 °F. In contrast, the temperature profile for Catalyst C at a higher (by 8 °F) sandbath temperature is nearly flat. The two test reactors have about the same nominal equivalent isothermal temperature defined as the arithmetic average of the measured temperatures along the bed.

There was no measurable movement of the hot spot toward the reactor outlet over the test period, indicating that catalyst deactivation is unimportant. Moreover, as Fig. 10 shows, the reactor bed temperature observed with NiMnMo drops back to the sandbath temperature near the reactor outlet, suggesting that the reaction may have stopped in that region. It is then

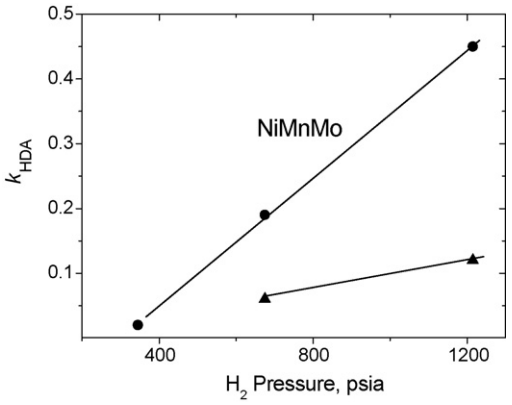

Fig. 9. Hydrodearomatization rate constants for bulk NiMnMo (●) and Catalyst C (▲) vs. hydrogen pressure. LCO, 650 °F, 0.86 LHSV, and 3000 SCF/B H_2.

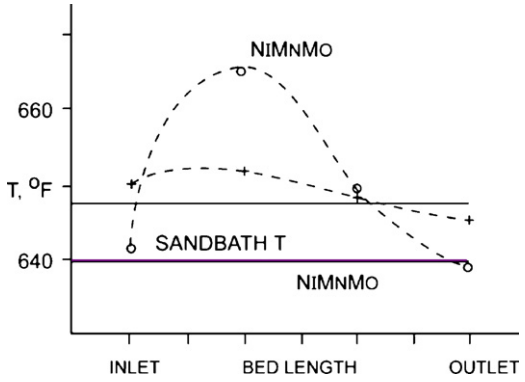

Fig. 10. Reactor axial temperature profiles for bulk NiMnMo (○) and Catalyst C (+). The sandbath temperature (horizontal line) for Catalyst C is 8 °F higher than that for NiMnMo.

reasonable to suspect that the catalyst in the downstream zone may not be fully utilized and that aromatics hydrogenation could have reached a pseudo-equilibrium. That the catalyst bed at 1200 psig may not be fully utilized is also consistent with the observation that both HDS and HDN are essentially complete. Due to the high hydrogenation activity of bulk sulfide catalysts, the possibility of a temperature excursion should be a major concern when operating a commercial adiabatic reactor [1].

6.2.2. Conversion of mononuclear aromatics

Table 4 shows that with either catalyst the hydrogenations of two- and three-ring aromatics (2R and 3R) are almost complete at 1200 psig, resulting in a significant increase in the concentration of 1R aromatics. Monoaromatics hydrogenation is known to be the bottleneck in the cascade hydrogenation of multi-ring aromatics [22,23]. How to enhance the activity of metal sulfide catalysts for 1R aromatics hydrogenation is a fertile research area. Note that conventional hydrotreating catalysts were largely developed for heteroatom removal, rather than for HDA.

The most notable difference between the two catalysts lies in the conversion of 1R aromatics, as shown in Tables 4 and 5. NiMnMo can convert both alkyl benzenes and tetralins, while Catalyst C cannot. With Catalyst C, the concentration of alkylbenzenes in the liquid product is higher than that in the feed. Presumably, this is due to heteroatom removal reactions as neither catalyst is expected to have a high ring-opening activity.

Model-compound studies on a commercial $NiMo/Al_2O_3$ catalyst have shown that the hydrogenation rate of tetralin is about twice that of *m*-xylene [24], consistent with that observed with unsupported MoS_2 [25]. This approximate two-fold reactivity difference was also observed in a study of jet fuel hydrogenation on a $NiMo/Al_2O_3$ catalyst [26].

Table 4
Aromatic ring distributions for feed and products

Liquid type	1R	2R	3R	Total	H/C
Feed	25.07	52.14	7.8	85.0	0.108
Catalyst C	79.16	1.56	0.02	80.7	0.125
NiMnMo	53.68	1.26	0.15	55.1	0.135

Table 5
Comparison of one ring aromatics conversion activities

Liquid type	Alkyl benzenes	Tetralins	Naphthalenes
Feed	12.06	11.6	38.2
Catalyst C	13.26	61.64	0.35
NiMnMo	9.05	42.2	0.26

The above results, taken together, indicate that the NiMnMo catalyst can perform the tough job of converting alkylbenzenes. Table 4 shows that NiMnMo produces a liquid product with a higher hydrogen content than Catalyst C. A high content of saturates is a processing objective of lube oil hydrotreating (Section 6.3).

As alluded to earlier, it is desirable to operate a highly hydrogenative bulk sulfide catalyst with a conventional catalyst in a stacked- or mixed-bed that plays the strength of each constituent catalyst in a synergistic fashion [15,27,28]. In so doing, one may also address the concern about temperature excursions.

For perspective, we remark that supported noble metal (e.g., Pt, Pd) catalysts are highly active for HDA; however, they are very sensitive to sulfur poisoning. On the other hand, conventional hydrotreating catalysts, while sulfur tolerant, are developed primarily for heteroatom removal and far less active than noble metal catalysts for HDA. Many MAM-derived bulk catalysts, such as NiMnMo, fall in between these two catalyst systems. The catalytically active sites on NiMnMo could have some metallic character.

6.3. Hydrotreating of lube basestocks

Besides a high HDN-to-HDS activity ratio, a major objective in lubricating oil refining is to increase viscosity index (VI) so the sensitivity of oil viscosity to temperature is low. Other processing objectives include lowering volatility and improving low-temperature properties. These require lube basestocks to have low contents of aromatics and naphthenics, and a high content of saturates. Linear paraffins in the lube boiling range have the highest VI (170–200), but negatively affect the product's low-temperature fluidity due to their high melting point. The second best family of compounds for VI are iso-paraffins whose VIs are in the 120–170 range. Alkylated naphthenes are third in the rank, with 110–140 VIs. Alkylated monoaromatics have somewhat lower VIs. Multi-ring compounds have unacceptably low VI, with multi-ring naphthenes at 20 or less, and multi-ring aromatics as low as −60. The distribution of molecular type in crude oils is such that the lube oil fractions often are rich in cyclic and unsaturated compounds. Catalytic hydroprocessing is the only viable option to convert low VI molecules to high VI products.

Experiments were conducted to test the bulk NiMnMo catalyst against a state-of-the-art commercial $NiMo/Al_2O_3$ catalyst on a partially dewaxed lube raffinate with a VI of 89. As Fig. 11 shows, the NiMnMo catalyst gives a higher VI over a wide temperature range. It should also be noted that NiMnMo significantly outperforms the commercial catalyst in terms of saturate content and nitrogen removal [16,29].

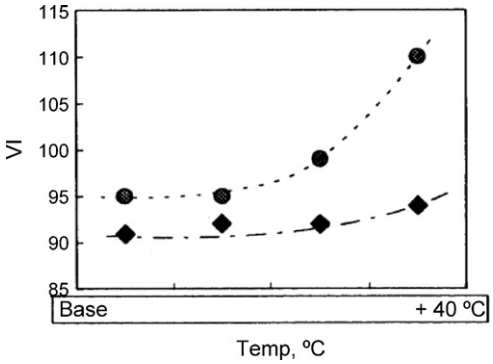

Fig. 11. Viscosity indexes (VI) for bulk NiMnMo (●) and commercial NiMo/Al_2O_3 catalyst (◆) vs. reactor temperature. Feed VI = 89.

6.4. Variants of MAM-derived catalysts

XPS studies indicated that promoter metals in bulk MAM-derived catalysts migrate to the catalyst surface during catalyst sulfiding [15]. This suggests a lack of "decoration sites" on MoS_2 edges for promoters. It may be desirable to lower the promoter-to-Mo ratio in the catalyst. This can be done by adding more Mo to existing MAM or replacing a portion of the promoters in MAM with "diluent" metals. Another way is to prepare the compound $[(ML)_xQ_{1-x}](MoO_4)$, with $0 < x < 1$ [15]. Here Q is the conjugate acid of the ligand L, with a charge sufficient to balance the dinegative charge of the metallate anion. For example, if L is en, then Q can be $[(H)_2(en)_3]^{+2}$, $[(H)_2(en)]^{+2}$, $[(H)_2(en)_2]^{+2}$ and mixture thereof. For convenience, catalysts derived from this class of precursors are called non-stoichiometric bulk sulfides [15].

Briefly, the salt $(ML)_xQ_{1-x}(MoO_4)$ can be prepared by dissolving the appropriate amounts of ammonium molybdate and an M-containing salt such as nitrate in an aqueous solution containing excess ligand L. The desired salt is precipitated by addition of a suitable antisolvent such as methanol or ethanol with agitation and is recovered by filtration. The XRD patterns show that the preparation does not lead to the formation of a physical mixture of $(ML)(MoO_4)$ and metallate salts of the form $Q(MoO_4)$. An example is $\{[Co(en)_3]_{0.75}Q_{0.25}\}(MoO_4)$, which upon decomposition and sulfiding is more active than NiMnMo in the HDS of 46DEDBT. The small MoS_2-like crystallites in this catalyst are largely present as single, double, and triple slabs, with an average number of stacking of 2.6 [15].

Finally, we mention that MAM materials, upon reduction with hydrogen at 200–400 °C, become highly active catalysts for HDA [30]. A synergistic effect was observed when two reduced MAM catalysts were used in a stacked bed.

7. Kinetic characterization of catalysts

In developing new hydroprocessing catalysts, one often needs to gain a deep understanding of the kinetic behaviors of these catalysts versus those of conventional catalysts. The art in kinetic characterization of promising experimental catalysts lies in balancing the need for fundamental understanding with that for practical relevance. This brings up the question of how best to integrate model-compound experiments into real-feed studies so that the results obtained from these two studies complement each other. It is important to design model-compound experiments based on information gathered from real-feed studies. We present two examples in sections to follow (Sections 7.1.2 and 7.2).

7.1. Catalyst–feedstock interactions

7.1.1. A real-world example

The example has to do with the development of a new HDN catalyst. Specifically, an experimental bulk catalyst, called Catalyst X, was tested with Feed I (a petroleum fraction) and found to be more active than a state-of-the-art commercial catalyst called Catalyst Y. It was also found that the rate data obtained with both catalysts could be fitted to first-order kinetics. Hence, Catalyst X's activity credit, in terms of savings in reactor volume, is the ratio of first-order HDN rate constants. The result was that Catalyst X showed a 40% activity advantage over Catalyst Y, regardless of the HDN level. This encouraging result raised the question of whether Catalyst X could have a broader application, which led to further tests with Feed II for a different application. Feed II has a much lower API gravity than Feed I. It has 740 wppm total nitrogen versus 705 wppm for Feed I.

Activity tests with Feed II showed that Catalyst X was better than Catalyst Y based on percent HDN removal at a fixed set of reaction conditions. The real question then is how much better Catalyst X is. There is no a priori reason why first-order kinetics can still be used for quantifying catalyst activity on Feed II. Kinetic experiments indicated that Catalyst X followed 0.8th-order kinetics, while Catalyst Y obeyed first order. Due to different reaction orders, Catalyst X's activity credit, determined as the reciprocal of the reactor volume ratio ($V_{cat\ Y}/V_{cat\ X}$), increases with increasing HDN level, as Fig. 12 illustrates. This activity credit curve is characterized by a relatively flat region (up to about 60% HDN) followed by a steep increase region. The credit varies between 1.5 and 1.6

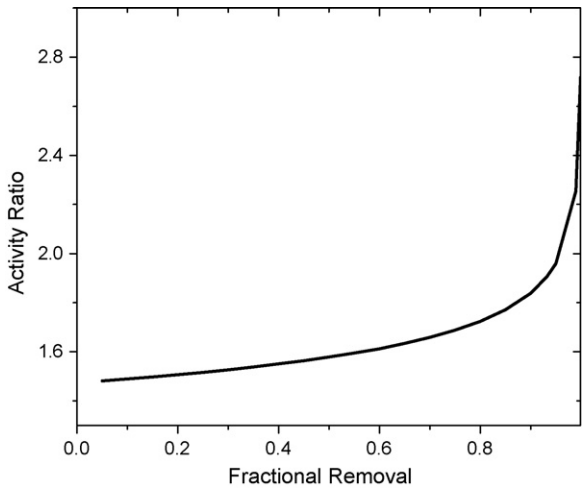

Fig. 12. Activity ratio (or reciprocal of reactor volume ratio) of Catalyst X to Catalyst Y vs. fractional HDN, Feed II.

over the flat region, which can be quickly estimated by taking the ratio k_X/k_Y where k_Y is the first-order rate constant for Catalyst Y and k_X an equivalent first-order rate constant for Catalyst X defined as $k_X = k_{0.8}N_f^{(0.8-1)}$, with $k_{0.8}$ and N_f being 0.8th-order rate constant and nitrogen feed concentration.

On the other hand, over the high HDN region (HDN > 60%), Catalyst X's activity credit is quite sensitive to the HDN level. For instance, it shows a 2.3-fold credit if the product nitrogen is lowered to 7 wppm. The underlying physics is that Catalyst X (0.8th-order kinetics) is more adsorptive than Catalyst Y (first-order kinetics), so its activity advantage increases with increasing percent HDN due to a diminishing self-inhibiting effect. A similar situation was encountered in the HDS of 46DEDBT over the bulk NiMnMo sulfide and a commercial catalyst [15].

This above ''cautionary tale'' points to the importance of obtaining kinetics at high conversions. Reactor size is extremely sensitive to kinetics at deep removal levels (say, >95%) except for zeroth-order kinetics. In the above example, Catalyst X outperforms Catalyst Y on both feeds. In practice, this may not necessarily be the case: catalyst ranking sometimes may reverse upon feed switching.

7.1.2. Model-compound studies

To probe why Catalyst X's activity credit becomes greater when switching over to Feed II, the compositions of nitrogen species in Feeds I and II were analyzed using electrospray ionization mass spectrometry (ESI-MS). Unlike the field desorption mass spectrometry, ESI-MS is selective toward the ionization of polar molecules. Our emphasis was on heterocyclic compounds because of their low HDN reactivity [15,31]. As Figs. 13 and 14 show, respectively, the nitrogen heterocycles in Feed I were found to be dominated by six-membered species such as quinolines, whereas those in Feed II are predominantly five-membered species such as carbazoles.

To gain more insights, side-by-side model-compound experiments were carried out to study the effect of hydrogen pressure on the HDN of quinoline (QN) versus that of 3-ethylcarbazole (3ECBZ) over a commercial $CoMo/Al_2O_3$-SiO_2 catalyst at 265 °C, 2.4 LHSV, and 650 SCF/B H_2 treat gas rate. The experimental setup was described elsewhere [32]. The total

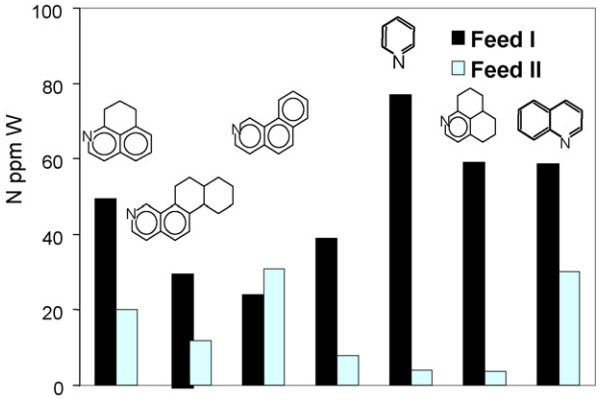

Fig. 13. Distributions of six-membered ring heterocycles in Feeds I and II determined by electrospray ionization mass spectrometry.

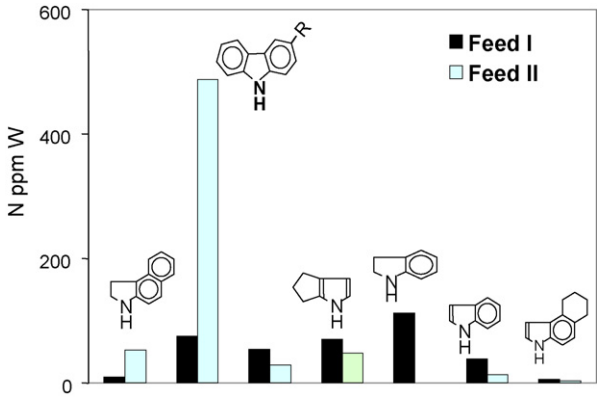

Fig. 14. Distributions of five-membered ring heterocycles in Feeds I and II determined by electrospray ionization mass spectrometry.

nitrogen concentration was kept constant at 574 wppm for both feeds. The catalyst was maintained in sulfide state with a sulfur-bearing compound in the feed.

Fig. 15 shows the results as percent HDN versus hydrogen pressure. While the curves connecting the data points are arbitrarily drawn rather than derived from correlation or modeling, the general trend is evident. The dependence of 3ECBZ HDN on hydrogen pressure is far stronger than that of QN HDN over the 400–450 psig pressure range. At low hydrogen pressures, the HDN rate of 3ECBZ is much lower than that of QN. At sufficiently high hydrogen pressures, the HDN rates become comparable and insensitive to H_2 pressure because the catalyst surface is saturated with adsorbed hydrogen. Hydrogenation reactions are generally more sensitive to hydrogen pressure than hydrogenolysis reactions [23]. Hence, Fig. 15 may be interpreted as indicating that the rate-limiting step in 3ECBZ HDN lies in hydrogenation, whereas that in QN HDN lies in hydrogenolysis. This interpretation is consistent with the results of previous HDN studies with 3ECBZ [31], QN [33], and real feeds [34].

In light of the above, we infer that Catalyst X is more hydrogenative than Catalyst Y. As a consequence, the activity

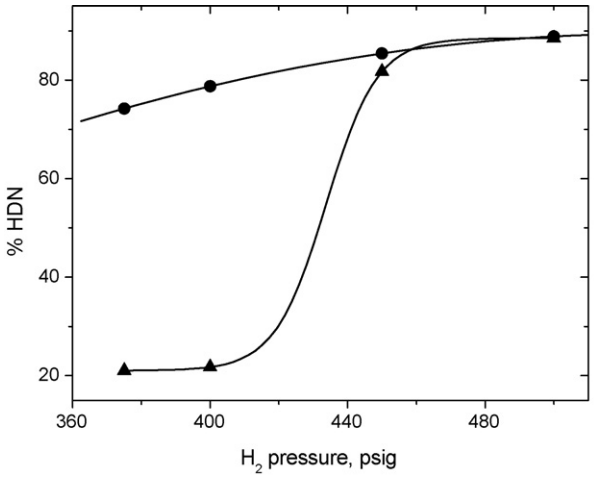

Fig. 15. Percent HDN of quinoline (●) and 3-ethylcarbazole (▲) vs. hydrogen pressure on a $CoMo/Al_2O_3$-SiO_2 catalyst at 265 °C, 2.4 LHSV, and 650 SCF/B H_2 treat gas rate.

credit of Catalyst X is bigger with Feed II whose treatment requires a relatively high hydrogenaton functionality. On the other hand, if the hydrogenolysis function of Catalyst X can be further enhanced without sacrificing its hydrogenation function, its activity credit for the HDN of Feed I would be higher than 40%. The key message here is that the relative HDN activities of these two catalysts depend on the relative amounts of five-membered and six-membered multi-ring nitrogen heterocycles in the feed.

Hydroprocessing catalyst development is to a large extent a matter of finding the optimum balance between hydrogenation and hydrogenolysis functionalities. The optimum balance depends on feedstock composition and operating conditions. Using bulk catalysts in combination with conventional supported catalysts offers an additional flexibility for process development. Recent advances in analytical techniques have made it possible to perform molecular speciation analyses on petroleum fractions for developing composition-based process models [35].

7.1.3. HDS–HDN interactions

We now consider another aspect of catalyst–feedstock interactions in the context of ultradeep HDS of middle distillates (200–370 °C boiling range). The selectivity trajectory analysis discussed in Section 3 shows how sulfur and nitrogen compounds compete with each other as their heteroatoms are being removed. Fig. 16 displays the trajectories for Catalysts X and Y with Feeds I and II through changes in LHSV at otherwise constant conditions. For Feed I, both catalysts move along essentially the same trajectory, with Catalyst X moving faster due to its higher activity. The same can be said of Feed II as well. This apparent "catalyst-invariant" behavior is surprising given that Catalysts X (bulk) and Y (supported) are very different. Apparently, in this case feedstock properties are the overriding factor governing the competition between HDS and HDN.

Referring to the curve for Feed II in Fig. 16, the trajectory initially moves from point F (feed) to point G in an approximately linear manner. Here the system is said to be in a low-interaction regime in that the HDS of reactive sulfur species is not seriously inhibited by nitrogen species. That is, nitrogen species are not formidable competitors. As the competition intensifies to a sufficiently high level (e.g., at low enough LHSVs), the trajectory then makes an abrupt turn and moves toward the HDN-selective region, from point G to point H. In this high-interaction regime, sulfur and nitrogen compounds "fight" fiercely for active sites. And nitrogen compounds "win" overwhelmingly as evidenced by the low slope of the trajectory between points G and H. For perspective, a hypercompetitive situation was observed in model-compound studies with 46DEDBT and 3ECBZ [32,36]: the trajectory is nearly horizontal ($p \approx 0$) [14].

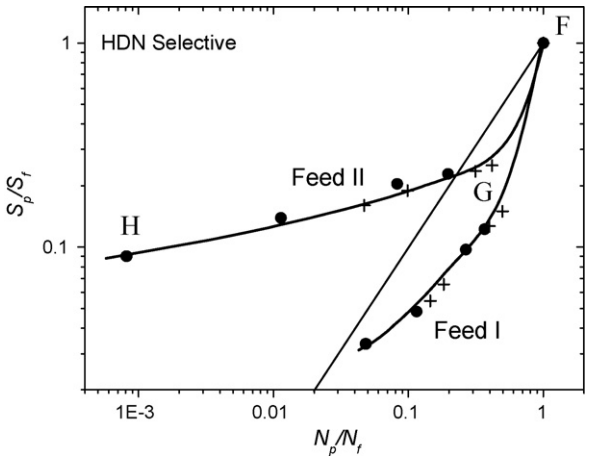

Fig. 16. HDN/HDS selectivity trajectories, $\ln(S_p/S_f)$ vs. $\ln(N_p/N_f)$, for Catalysts X (●) and Y (+) on Feeds I and II. The straight line means equal selectivity.

The trajectory for Feed I shows the same qualitative feature: it becomes more and more curved toward the HDN-selective region as the HDS level gets deeper due to increasing nitrogen inhibition. However, the properties of Feed I and the reaction conditions are such that the trajectory does not cross the parity line. In any event, both trajectories (Feeds I and II) are concave upward, meaning that sulfur compounds progressively lose the competitive adsorption battle against nitrogen compounds. Note that partially hydrogenated nitrogen heterocycles are likely more poisonous than their parent molecules [15,31].

By contrast, the trajectories of bulk FeMo and CrMo sulfides (Fig. 2) lie in the HDN-selective region owing to the catalysts' high selectivity toward HDN. As the asymptotic analysis predicts (Eq. (6)), their trajectories tend to be linear. The straight-line trajectory of the $NiMo/Al_2O_3$ catalyst in Fig. 2 is largely due to the fact that the reaction conditions are insufficiently severe to reach the high-interaction regime. As an aside, Fig. 16 is a selectivity plot without explicit information on reaction rates. To incorporate kinetics information and take advantage of the catalyst-invariant feature of the system, one can superimpose a 1/LHSV versus $\ln(N_p/N_f)$ plot on Fig. 16 for each of the two catalysts.

7.2. Catalytic characterization in the high-interaction regime

A conclusion from preceding sections is this: removing the last bit of sulfur will be fiercely "opposed" by nitrogen compounds. Consistent with this are observations made in two early studies. In the not-so-deep-HDS of raw distillates, the organonitrogen inhibiting effect is small, even less important than organosulfur self-inhibiting effect [37]. On the other hand, the HDS reactivity of prehydrotreated middle distillates is primarily governed by the feed nitrogen content [38].

Many difficult-to-desulfurize middle distillates have significant amounts of carbazoles, which cannot compete with six-membered heterocycles for catalytically active sites. As a result, they usually survive hydrotreating. This is why in the GC traces of hydrotreated products, there often exist clusters of peaks referred to as the "carbazole envelope" [39,40]. Some of the carbazole type compounds are partially hydrogenated and likely more poisonous than their parent molecules.

The foregoing discussions help define a natural "boundary condition" for ultradeep HDS of middle distillates, which led to

the experimental and modeling studies using 46DEDBT and 3ECBZ as model compounds [14,32,36]. Indeed, the inhibiting effect of 3ECBZ is far more pronounced in the HDS of 46DEDBT than that of DBT [32]. We next briefly describe how these studies were done and highlight some conclusions.

The majority of past efforts to quantify the competitive chemisorption effects were based on steady state experiments using quantitatively incomplete or oversimplified kinetic models. For example, one often uses the following Langmuir–Hinshelwood kinetic model without justification

$$r_{\mathrm{HDS}} = \frac{(k_{\mathrm{HDS}}K_s q)S^n P_{\mathrm{H}}^m}{1 + K_n N + K_s S + K_a A} = \frac{k_s S^n P_{\mathrm{H}}^m}{1 + K_n N + K_s S + K_a A} \tag{10}$$

where k_{HDS}, K_s, and q are surface HDS rate constant, sulfur adsorption equilibrium constant, and total active site density, respectively. In practice, they are lumped into a single parameter $k_s = k_{\mathrm{HDS}}K_s q$ for expediency, and only k_s is determined experimentally. This lumped rate parameter k_s is often correlated with the structure of hydrocarbon molecules [35]. Note that the denominator may also include additional inhibition terms due to, say, H_2S. An implicit assumption here is fast adsorption–desorption equilibrium, so the overall rate is limited by surface reactions.

Pitfalls may arise when applying the above approach indiscriminately for catalytic characterization of promising experimental catalysts that are vastly different from conventional catalysts. The assumption of fast equilibrium is reasonable for some catalysts, but may be untenable for others. Moreover, take bulk NiMnMo sulfide and a conventional $CoMo/Al_2O_3$ catalyst, the essential difference between the two catalysts may well lie in q. In this and similar cases, the experiments should be designed to extract q.

The above situation can be rectified by conducting quantitative mechanism-based experiments under transient conditions using properly chosen model compounds. Such experiments entail tracking changes in system behavior following an imposed perturbation. Specifically, the results to be discussed were obtained from a perturbation in the form of a step function. That is, HDS experiments were started with a feed containing 46DEDBT to obtain the base-case data in the absence of an organonitrogen inhibitor. After the catalyst lined out its activity in a fixed-bed flow reactor (steady state I), the feed was switched over to one that contains 46DEDBT and 3ECBZ at the same reaction conditions. The state of the reactor is monitored by intermittently analyzing the liquid products at the reactor outlet until the catalyst reached a new steady state (steady state II). Modeling the thus-obtained data offers an effective means of discriminating among rival models [14,36]. As an aside, a sudden introduction of an isotopically labeled species such as [^{35}S]DBT or [^{35}S]H_2S has been used to probe the nature of active sites [41].

Mathematical models have been developed [14,36] to interpret the data obtained during the transient breakthrough period and at the two steady states (I and II). The nomenclature for the models is as follows. For sulfur species, k_s, k'_s, and k_{HDS} are the adsorption constant, desorption constant, and surface HDS rate constant, respectively. The corresponding rate constants for nitrogen species are k_n, k'_n, and k_{HDN}. The fractional coverages of adsorbed nitrogen and sulfur are θ_n and θ_s, respectively, defined as $\theta_n = q_n/q$ and $\theta_s = q_s/q$ where q_n and q_s are the adsorbed nitrogen atom and adsorbed sulfur atom concentrations. The HDS and HDN rates at constant hydrogen pressure under competitive chemisorption environment are

$$r_{\mathrm{HDS}} = \frac{(k_{\mathrm{HDS}}k_s q/\kappa_s)S}{1 + k_n N/\kappa_n + k_s S/\kappa_s} \tag{11}$$

$$r_{\mathrm{HDN}} = \frac{(k_{\mathrm{HDN}}k_n q/\kappa_n)N}{1 + k_n N/\kappa_n + k_s S/\kappa_s} \tag{12}$$

where $\kappa_n \equiv k'_n + k_{\mathrm{HDN}}$ and $\kappa_s \equiv k'_s + k_{\mathrm{HDS}}$. The selectivity factor is $p = k_s k_{\mathrm{HDS}}\kappa_n/(k_n k_{\mathrm{HDN}}\kappa_s)$.

While the model encompasses many time scales, seldom does the need for considering all of them arise. The key is to identify kinetically important steps over the time scale of interest through controlled transient and steady state experiments. The classical Langmuir–Hinshelwood equilibrium model corresponds to $k'_s \gg k_{\mathrm{HDS}}$ and $k'_n \gg k_{\mathrm{HDN}}$. It turns out that the 46DEDBT-3ECBZ competitive chemisorption experiments corresponds to $k'_n \ll k_{\mathrm{HDN}}$, $k'_s \ll k_{\mathrm{HDS}}$, and $k_{\mathrm{HDS}} \gg k_s S_{\mathrm{f}}$ [14,36]. Since sulfur self-inhibition is relatively insignificant, it is reasonable to set $k'_s \gg k_s S_{\mathrm{f}}$.

We have used the foregoing approach to characterize promising bulk catalysts versus conventional catalysts. For illustration, we discuss some results obtained with a conventional $CoMo/Al_2O_3$-SiO_2 catalyst in the 46DEDBT–3ECBZ experiments [14]. Fig. 17 shows the observed percentage of HDS and effluent nitrogen concentration (ppmw atom) after a sudden step change in the feed nitrogen content from zero to 80 ppmw at time zero. The solid curves are model predictions. A high HDS level of 70% is achieved prior to time zero (steady state I), after which the percent HDS declines as the nitrogen

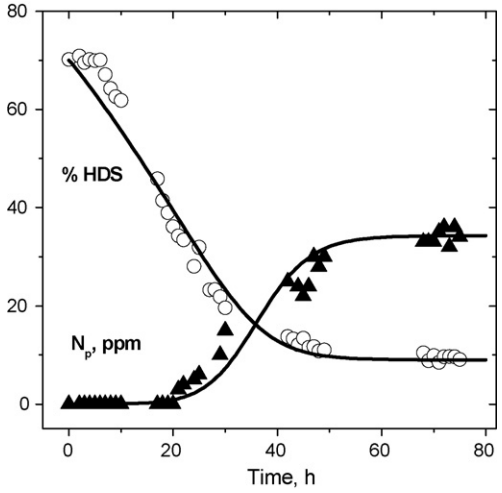

Fig. 17. Percentage HDS of 46DEDBT (○) and nitrogen concentration (▲) in liquid effluent at the reactor exit vs. elapsed hour after introduction of 3-ethylcarbazole; $CoMo/Al_2O_3$-SiO_2 catalyst, 265 °C, 2.4 LHSV, 1.83 MPa, and 116 cc H_2/cc liquid feed. The solid curves are model predictions.

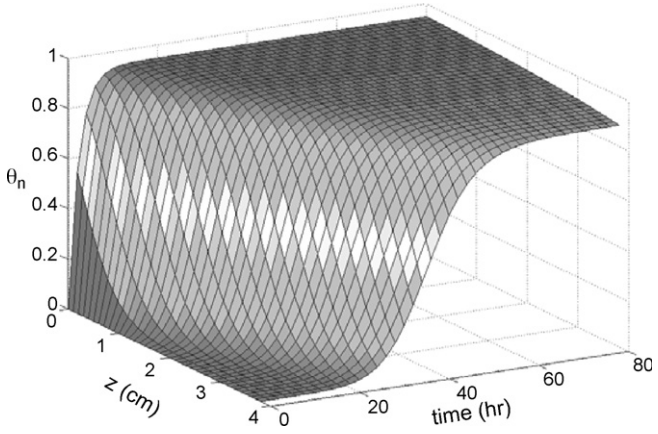

Fig. 18. Predicted spatial and temporal variation of θ_n, the fractional site coverage by adsorbed nitrogen. HDS of 46DEDBT and HDN of 3ECBZ.

poison front moves towards the reactor exit. The breakthrough of the nitrogen species does not occur until after 20 h. After this point the nitrogen content of the liquid effluent starts to rise, eventually giving rise to a steady state HDN level of 58%. The percentage of HDS at steady state II is about 10%.

Fig. 18 shows the spatiotemporal behavior of θ_n, which increases sharply and then levels off at the reactor inlet ($z = 0$). At $t = 0$ h, the catalyst bed is preadsorbed with sulfur species, with θ_s decaying exponentially along the reactor as shown in Fig. 19. As nitrogen species arrive ($t > 0$), sulfur species start to give up their ''adsorption seats'' near the entrance. The sulfur species in the fluid phase then have to go further downstream to ''fish'' for bare active sites. As a result, the maximum in θ_s moves from the reactor inlet toward the bed interior and reaches the reactor outlet. An observer standing at the reactor outlet will notice that $\theta_s(t)$ goes through a maximum as time goes by.

The picture that emerges is that 46DEDBT and 3ECBZ have vastly different adsorptivities and reactivities. A small fraction of the active sites give a high 70% HDS at steady state I versus a 58% HDN over a lot of active sites at steady state II. Thus, the surface turnover rate for the HDS of 46DEDBT is far greater than that for the HDN of 3ECBZ. Compared with 3ECBZ, 46DEDBT has a much weaker affinity for active sites. The

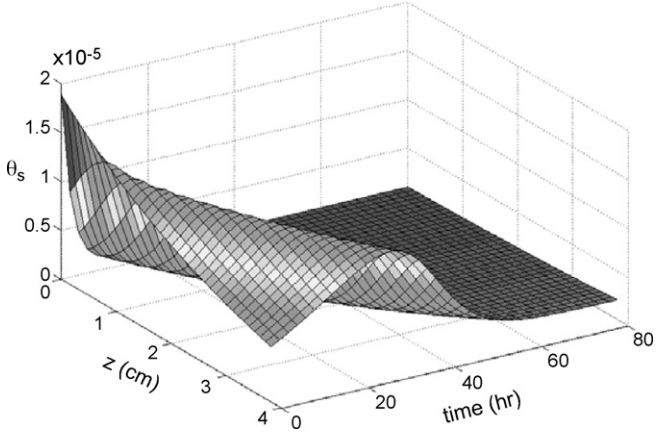

Fig. 19. Predicted spatial and temporal variation of θ_s, the fractional site coverage by adsorbed sulfur. HDS of 46DEDBT and HDN of 3ECBZ.

catalyst can adsorb 3ECBZ at a rate at least 17-fold faster than it can denitrogenate 3ECBZ. All the seven parameters (k_s, k'_s, k_{HDS}, k_n, k'_n, k_{HDN}, and q) that characterize the catalyst under reaction conditions were determined [14], which can be contrasted with those obtained with experimental catalysts.

7.3. Meaning of reaction order

Power-law kinetic models have widely been used for catalyst development. Catalysts X and Y in Section 7.1 have different HDN reaction orders, which make catalyst ranking more involved. Here we briefly discuss the meanings of the reaction order in the context of feedstock–catalyst interactions.

The problem to be addressed can be stated as follows. Let $c_i(t; c_{if,})$ be the concentration of the ith reactant (say, an organosulfur species) and c_{if} be its concentration in the feed mixture. Each reactant disappears at the rate r_i. The total concentration is $C(t) = \Sigma_i c_i$. The task is to find an overall kinetics $R(C)$ for the mixture as a whole, that is, LHSV$(\mathrm{d}C/\mathrm{d}\tau) = -R(C)$ for a plug-flow reactor. The form of $R(C)$ depends on r_i and how c_{if} distribute among themselves in the feed. If $R(C) = \bar{k}C^n$, then n is the overall reaction order. Given the astronomically large number of reacting species in a petroleum mixture, it pays to treat the mixture as a continuum [42,43]. The continuum approach has produced a large body of pragmatically useful results that help explain some intriguing kinetic behaviors observed in hydroprocessing [35,44]. Examples: (a) high-activity catalysts give rise to lower overall order than low-activity catalysts; (b) refractory feeds show higher overall order than reactive ones; (c) the overall HDS order decreases with increasing temperature; (d) the overall order for HDS is higher than that for HDN, and (e) the overall order for the plug-flow reactor is higher than that for the continuous stirred tank reactor.

Experiments using model compounds have indicated that the individual HDS rate in most cases is pseudo-first order [23]. Consider a first-order reaction mixture, we use the rate constant k as the reactant label (replacing i with k). In the continuum approach, the total concentration $C(t)$ is expressed as an integral instead of a sum, namely,

$$C(t) = \int_0^\infty c_\mathrm{f}(k) \exp(-kt)\mathrm{d}k \tag{13}$$

where $c_\mathrm{f}(k)\mathrm{d}k$ is the reactant concentration in the feed with k between k and $k + \mathrm{d}k$. Now consider the case where the feed can be described by the gamma distribution [42–44]

$$c_\mathrm{f}(k) = \chi^\chi \left(\frac{k}{\bar{k}}\right)^{\chi-1} \frac{\exp(-\chi k/\bar{k})}{\bar{k}\Gamma(\chi)}, \quad \chi > 0 \tag{14}$$

where Γ is the gamma function. With two parameters, $\bar{k}$ and χ, $c_\mathrm{f}(k)$ can portray a wide variety of feed properties [6,44]. The smaller the χ value, the more refractory is the feed. When $\chi = 1$ the distribution is exponential, indicating that the feed contains a finite amount of nearly unconvertible species. If $\chi > 1$, the distribution is monomodal. Eq. (14) can indeed describe many petroleum properties [45–47]. It follows from Eqs. (13) and (14) that for a plug-flow reactor [42,43], the overall kinetics is

nth-order with an overall rate constant $\bar{k}$

$$R(C) = \bar{k}C^n, \quad n = 1 + \frac{1}{\chi} \tag{15}$$

This expression for the overall kinetics relates macroscopic behavior to microscopic details of the feed. The mixture behaves like a single species with a higher-than-first-order kinetics. Since the analysis does not consider competitive chemisorption, all the inhibiting effects and hydrogen pressure are incorporated into $\bar{k}$. A short interpretation of the higher overall order is that as reaction time increases, the reactive species disappear rapidly and the mixture becomes progressively more refractory. The discussions in preceding sections offer a physically more clear explanation, namely that the removal of sulfur becomes increasingly more inhibited by nitrogen compounds as the HDS level gets deeper, resulting in a high-order apparent kinetics.

Referring to Eq. (15), when the reactivity spread is broad (small χ), n is high. When the spread becomes narrow, $R(C)$ approaches first order. Eqs. (14) and (15) explain a commonly observed phenomenon parsimoniously: that a refractory feed (e.g., $\chi = 1$) gives a higher overall order than a reactive one (e.g., $\chi = 1.5$). It is useful to correlate χ with feed properties such as specific gravity, nitrogen content, etc. [48]. The literature abounds with examples of higher-than-first-order HDS kinetics for various petroleum fractions.

It is customary in catalyst exploratory studies to evaluate a wide variety of experimental catalysts with a standard feed. A catalyst that does not activate certain refractory components of the feed might well be evaluated by, say, second-order kinetics. But if the catalyst preparation is improved so part of the refractory components can be attacked, then an overall order less than two would have to be used in evaluating the improved catalyst. In process research, it is common to run different feeds on a selected catalyst over a wide range of conditions. The overall reaction order increases when switching from an ''easy'' feed to a ''hard'' feed. The extent of this increase may be viewed as an index of feed refractoriness. The overall order is expected to increase with decreasing reaction severity. In summary, the overall order n is an indicator of the following: (1) whether or not the catalyst is active enough to activate the most refractory species or (2) whether or not the conditions are severe enough to convert the least reactive species.

Some examples from the literature are helpful. The overall HDS order increases from 1.5 to 2 when switching from a blend of light coker gas oil and virgin gas oil to LCO [49]. In the HDS of middle distillates, the overall order increases with feedstock's sulfur content [50]. Also, the HDS order increases from 2.2 to 3.8 as the relative concentration of refractory sulfur species becomes disproportionately large [51]. Increasing the reaction severity results in a decrease in the overall order; examples include increasing temperature [52] and removing H_2S [47]. Modifying the acidity of hydroprocessing catalyst supports can change the overall order n [53].

Now turn to the bulk catalysts of the present study. Doubly-promoted MAT type catalysts, being more active than conventional catalysts for the HDS of LCO, show an HDS order of 1.5, versus second order for conventional catalysts [6]. The HDN orders for Catalysts X (bulk) and Y (supported) on Feed II are, respectively, 0.8 and 1 (Section 7.1.1). On this point, we remark that the HDN of individual nitrogen compounds is often describable by zero- or near-zero-order kinetics due to strong adsorption [54,55]. It has been shown that the overall order of many zeroth-order reactions is higher than zero and can be as high as two if the feed contains a high concentration of really refractory nitrogen compounds [56].

8. Concluding remarks

An essential step toward developing new or improved hydroprocessing catalysts is gaining a better control of catalyst functionalities (hydrogenation versus hydrogenolysis) and a better understanding of catalyst–feedstock interactions. To this end, this article describes an integrated approach consisting of (1) developing new synthesis chemistries, (2) conducting model-compound experiments alongside real-feed kinetic studies, and (3) characterizing catalysts and feedstocks.

The emphasis of this article is on bulk and dispersed sulfide catalysts prepared from two families of molecular complexes. Compared with conventional catalysts, these catalysts are unusually selective toward HDN, highly hydrogenative, more sensitive to hydrogen pressure, and intrinsically more active for the HDS of 4-substituted and 4,6-disubstituted dibenzothiophenes. They show a pronounced effect of metal composition. Their high selectivity for HDN opens the door to exploitation of hitherto inaccessible region of the HDS–HDN space. This led to the discovery of the following pairs of synergistic copromoters: Ni-Mn and Cr-Fe. The high hydrogenation activities of bulk sulfide catalysts can potentially give rise to temperature excursion in a commercial reactor. To maximize the benefit-to-cost ratio and achieve better control of reaction exothermicity, some highly hydrogenative bulk catalysts should be used in combination with a conventional catalyst in a stacked bed.

After activation and sulfiding, molecular-complex-derived catalysts generally retain certain amounts of carbon- and nitrogen-containing species, which may also be a contributing factor to their unusual activity and selectivity. There are good discussions on the role of carbonaceous species in hydroprocessing catalysis [57,58]. Some bulk sulfide catalysts, such as MAT-derived FeMo and CrMo, are basically amorphous in nature with MoS_2-like structure having just one or two layers.

Acknowledgements

Thanks are due to R.R. Chianelli, A.J. Jacobson, S.L. Soled, A. Moreland, A.R. Young, W.-H. Pan, K. Qian, H. Murray, and R. Krycak.

References

[1] S. Eijsbouts, S.W. Mayo, K. Fujita, Appl. Catal. 322 (2007) 58.
[2] T.C. Ho, A.R. Young, A.J. Jacobson, R.R. Chianelli, US Patent 4,632,747 (1986).

[3] A.J. Jacobson, T.C. Ho, R.R. Chianelli, T.A. Pecoraro, US Patent 4,666,878 (1987).
[4] T.C. Ho, R.R. Chianelli, A.J. Jacobson, A.R. Young, US Patent 4,698,145 (1987).
[5] T.C. Ho, A.J. Jacobson, R.R. Chianelli, C.R.F. Lund, J. Catal. 132 (1992) 351.
[6] T.C. Ho, A.J. Jacobson, R.R. Chianelli, Appl. Catal. 114 (1994) 127.
[7] T.C. Ho, Ind. Eng. Chem. Res. 32 (1993) 1568.
[8] T.C. Ho, R.R. Chianelli, W.H. Pan, A.J. Jacobson, AIChE Meeting, Houston, Texas, March 19–23, 1995.
[9] T.C. Ho, A.R. Young, R.R. Chianelli, A.J. Jacobson, US Patent 4,519,429 (1986).
[10] A.R. Young, T.C. Ho, A.J. Jacobson, R.R. Chianelli, US Patent 4,749,673 (1988).
[11] R.R. Chianelli, T.C. Ho, A.J. Jacobson, A.R. Young, US Patent 4,748,142 (1988).
[12] H.T. Hall, H. Eyring, J. Am. Chem. Soc. 72 (1950) 782.
[13] H. Topsøe, B.S. Clausen, F.E. Massoth, Hydrotreating Catalysis, Springer-Verlag, 1996.
[14] T.C. Ho, D. Nguyen, Chem. Eng. Commun. 193 (2006) 460.
[15] T.C. Ho, Catal. Today 98 (2004) 3.
[16] D.T. Eadie, M.A. Fefer, US Patent 5,122,258 (1992).
[17] J.Y. Koo, T.C. Ho, Catal. Lett. 28 (1994) 99.
[18] T.C. Ho, L.E. McCandlish, US Patent 4,595,672 (1986).
[19] T.C. Ho, S.C. Reyes, Chem. Eng. Sci. 45 (1990) 2633.
[20] S.C. Reyes, T.C. Ho, AIChE J. 34 (1988).
[21] T.C. Ho, J. Catal. 131 (1991) 298.
[22] A. Stanislaus, A.H. Cooper, Catal. Rev.-Sci. Eng. 36 (1994) 75.
[23] M.J. Girgis, B.C. Gates, Ind. Eng. Chem. Res. 30 (1991) 2021.
[24] T.C. Ho, Energy Fuels 8 (1994) 1149.
[25] O. Weisser, S. Landa, Sulfided Catalysts, Their Properties and Applications, Pergamon Press, 1973.
[26] L.M. Magnabosco, in: D.L. Trimm, S. Akashah, M. Absi-Halabi, A. Bishara (Eds.), In Studies in Surface Science and Catalysis, vol. 53, Elsevier, New York, 1990.
[27] T.C. Ho, US Patent 4,902,404 (1990).
[28] T.C. Ho, US Patent 4,973,397 (1990).
[29] A. Ravella, I.A. Cody, T.C. Ho, M. Daage, Proc. 44th Canadian Chem. Eng. Conf., 1994.
[30] T.C. Ho, C.R. Symon, V. Buchholz, M. Daage, US Patent 5,767037 (1998).
[31] T.C. Ho, Catal. Rev.-Sci. Eng. 30 (1988) 117.
[32] T.C. Ho, J. Catal. 219 (2003) 442.
[33] S.H. Yang, C.N. Satterfield, Ind. Eng. Chem., Proc. Des. Dev. 23 (1984) 20.
[34] S.K. Bej, A.K. Dalai, J. Adjaye, Energy Fuels 15 (2001) 377.
[35] T.C. Ho, in: C.S. Hsu, P.R. Robinson (Eds.), Practical Advances in Petroleum Processing, vol. 2, Springer, 2006.
[36] T.C. Ho, D. Nguyen, J. Catal. 222 (2004) 450.
[37] T.C. Ho, Appl. Catal., A: Gen. 244 (2003) 115.
[38] T.C. Ho, G.E. Markley, Appl. Catal., A: Gen. 267 (2004) 245.
[39] C.W. Hudson, US Patent 4,591,430 (1986).
[40] A.O.I. Krause, M. Joutsimo, Ketjen Catalysts Symposium, H-2, 1986.
[41] T. Kabe, A. Ishihara, W. Qian, Hydrodesulfurization and Hydrodenitrogenation, Wiley–VCH, New York, 1999.
[42] R. Aris, Arch. Ratl. Mech. Anal. 27 (1968) 356.
[43] T.C. Ho, R. Aris, AIChE J. 33 (1987) 1050.
[44] T.C. Ho, in: B. Delmon, G.F. Froment, P. Grange (Eds.), Hydrotreatment and Hydrocracking of Oil Fractions, Elsevier, 1999.
[45] C.H. Whitson, Soc. Pet. Eng. J. 12233 (1983) 683.
[46] S.K. Shibata, S.I. Sandler, Chem. Eng. Sci. 42 (1987) 1977.
[47] R. Stephan, G. Emic, H. Hoffman, Chem. Eng. Process. 19 (1985) 303.
[48] S. Inoue, T. Takatsuka, Y. Wada, S. Hirohama, T. Ushida, Fuel 79 (2000) 843.
[49] J.W.M. Sonnemans, Ketjen Catalyst Symposium, 1982.
[50] J. Ancheyta, M.J. Angeles, M.J. Macias, G. Marroquin, R. Morales, Energy Fuels 16 (2002) 189.
[51] M. Breysse, G. Djega-Mariaassou, S. Pessayre, C. Geantet, M. Vrinat, G. Perot, M. Lemaire, Catal. Today 84 (2003) 129.
[52] H. Ozaki, Y. Satomi, T. Hisamitsu, Proc. 9th World Petroleum Congress vol. 18, 4, 1976, 6 PD.
[53] A.L. Hensley Jr., A.M. Tait, J.T. Miller, T.D. Nevitt, US Patent 4,406,779 (1983).
[54] C.M. Smith, C.N. Satterfield, Chem. Eng. Sci. 41 (1986) 839.
[55] J.T. Miller, M.F. Hineman, J. Catal. 85 (1984) 117.
[56] T.C. Ho, B.S. White, R. Hsu, ALChE J. 36 (1990).
[57] R. Prins, V.H.J. DeBeer, G.A. Somorjai, Catal. Rev.,-Sci. Eng. 31 (1989) 1.
[58] S.P. Kelty, G. Berhault, R. Chianelli, Appl. Catal. A: Gen. 322 (2007) 9.